Remote Sensing of Environment 237 (2020) 111535

Contents lists available at ScienceDirect

Remote Sensing of Environment

journal homepage: www.elsevier.com/locate/rse

Evaluation of pushbroom DAP relative to frame camera DAP and lidar for forest modeling

Jacob L. Strunk[a,*], Peter J. Gould[b], Petteri Packalen[c], Demetrios Gatziolis[d], Danuta Greblowska[e], Caleb Maki[f], Robert J. McGaughey[g]

[a] USDA Forest Service Pacific Northwest Research Station, 3625 93rd Ave SW, Olympia, WA, 98512, USA
[b] Washington State Department of Natural Resources, PO Box 47000, 1111 Washington Street, SE, Olympia, WA, 98504-7000, USA
[c] School of Forest Sciences, Faculty of Science and Forestry, University of Eastern Finland, P.O. Box 111, 80101, Joensuu, Finland
[d] USDA Forest Service Pacific Northwest Research Station, 620 Southwest Main, Suite 502, Portland, OR, 97205, USA
[e] GeoTerra Inc., 60 McKinley St, Eugene, OR, 97402, USA
[f] Washington State Department of Natural Resources, PO Box 47000, 1111 Washington Street SE, Olympia, WA, 98504-7000, USA
[g] USDA Forest Service Pacific Northwest Research Station, University of Washington, PO Box 352100, Seattle, WA, 98195-2100, USA

ARTICLE INFO

Keywords:
Lidar
Structure from motion
Photogrammetry
Forestry
DAP
Pushbroom
Frame-camera
Forest inventory
Forest modeling
Point cloud
NAIP

ABSTRACT

There is growing interest in using Digital Aerial Photogrammetry (DAP) for forestry applications. However, the performance of pushbroom DAP relative to frame-based DAP and airborne lidar is not well documented. Interest in DAP stems largely from its low cost relative to lidar. Studies have demonstrated that frame-based DAP generally performs slightly poorer than lidar, but still provides good value due to its reduced cost. In the USA pushbroom imagery can be dramatically less expensive than frame-camera imagery in part because of a nationwide collection program. There is an immediate need then to understand how well pushbroom DAP works as an auxiliary data source in the prediction of key forest attributes including basal area, volume, height, and the number of trees per ha.

This study compares point clouds generated from 40 cm pushbroom DAP with point clouds from lidar and 7.5 cm, 15 cm, and 30 cm frame-based DAP. Differences in point clouds from these data sources are readily apparent in visual inspections; e.g. DAP tends to measure canopy gaps poorly, omit individual trees in openings, is typically unable to represent the ground beneath canopy, and is susceptible to commission errors manifested as points above the canopy surface. Frame-based DAP provides greater canopy detail than pushbroom DAP, which becomes more apparent with higher image resolution. Our results indicated that DAP height metrics generally have a strong linear relationship with lidar metrics, with R^2 values ranging from 83 – 90% for cover, and 47–80% for height quantiles. Similarly, lidar auxiliary variables explain the greatest variation in forest attributes, e.g., volume (84%), followed closely by 30 cm frame-based DAP (81%), with the poorest results from pushbroom DAP (75%). While DAP resolution had a visible effect on canopy definition, it did not appreciably affect point cloud metrics or model performances. Although pushbroom DAP explained the least variation in forest attributes, it still had sufficient explanatory power to provide good value when frame-based DAP and lidar are not available.

1. Introduction

There is growing interest within the forestry community in airborne remote sensing technologies that can measure vertical forest structure, such as lidar, radar, and Digital Aerial Photogrammetry (DAP; also commonly Structure From Motion or, colloquially, phodar). Orthophotos are the most common way that people interact with DAP products, although here we only discuss DAP derived point clouds. The technologies mentioned enable the users to quantify fine-scale variation in forest attributes (e.g. volume and biomass; Strunk et al., 2012) whereas conventional imagery alone requires a less direct (and usually less precise) inference from 2D patterns to 3D structure. Lidar is

* Corresponding author.
E-mail addresses: Jacob.Strunk@usda.gov (J.L. Strunk), Peter.Gould@dnr.wa.gov (P.J. Gould), Petteri.Packalen@uef.fi (P. Packalen), Demetrios.Gatziolis@usda.gov (D. Gatziolis), DGreblowska@GeoTerra.us (D. Greblowska), Caleb.Maki@dnr.wa.gov (C. Maki), Bob.McGaughey@usda.gov (R.J. McGaughey).

https://doi.org/10.1016/j.rse.2019.111535
Received 9 May 2019; Received in revised form 1 November 2019; Accepted 10 November 2019
0034-4257/ Published by Elsevier Inc.

arguably the most reliable and precise operational source of remotely sensed vegetation structure measurements, but its cost has proven to be an impediment to its extensive and repeated use in forest inventory. For example, according to the 2019 United States Interagency Elevation Inventory, a large proportion of the western half of the USA has not been covered by lidar, while the entire conterminous USA is covered regularly with imagery, e.g. every 2–3 years by the National Agriculture Imagery Program (NAIP). In studies using frame-based DAP (the NAIP program uses pushbroom imagery), DAP was shown to provide slightly less explanatory power than lidar (e.g. White et al., 2015a), but can be much more cost-effective than lidar, facilitating integration with repeated forest inventory.

Advances in forest monitoring with airborne DAP can dramatically improve the spatial and temporal resolutions of forest monitoring information for the conterminous USA. This is an important consideration given recent concerns over widespread declines in forest health related to air temperature, droughts, insects, pathogens, and fires (Allen et al., 2010; Anderegg et al., 2013; Haavik et al., 2015; Jactel et al., 2012; Mantgem et al., 2013; Millar and Stephenson, 2015). Studies such as White et al. (2015) and Vastaranta et al. (2014) have shown that DAP derivatives can be used to model forest conditions such as height, basal area, volume, biomass, and other associated attributes indicative of forest health, fire risk, or the severity impacts from mortality and fire (e.g. amount of carbon released). This type of information is already available nationwide for the USA, mostly in tabular format, from field data collected and distributed by the Forest Inventory and Analysis (FIA) program. Deriving this information from DAP would enable transition from FIA's nominal ground sample distance of approximately 5 km to seamless mapped predictions (e.g. $R^2 > 0.7$ for volume from pushbroom DAP in Strunk et al., 2019) with better than 30 m resolution for the set of forest attributes which can be predicted effectively with DAP. This makes the pushbroom imagery used for the NAIP program a compelling resource to improve the quality of nationwide forest maps and small-area estimates. However, the cost of imagery varies widely with acquisition specifications that also affect the suitability of DAP for forest inventory applications.

While the low cost of DAP relative to lidar has the potential to increase the viability of remotely-measured forest structure as a tool for forest inventory, the tradeoffs between different image acquisition specifications are not clear. Studies have looked at the utility of DAP for forest inventory assessments using imagery ranging from at least 13 cm (Iqbal et al., 2019) to 2 m (Pearse et al., 2018), with different amounts of overlap (Bohlin et al., 2012), small format cameras (Puliti et al., 2015), medium format cameras (Iqbal et al., 2019), large format cameras (Kangas et al., 2018), and even space-borne sensors (Immitzer et al., 2016). The effects of image matching algorithm (Kukkonen et al., 2017) and software implementation (Probst et al., 2018) have also been compared. Several studies have started to unravel the implications of differences in acquisition specifications on the suitability of DAP for forestry including, e.g., Kangas et al. (2018) took images from a single acquisition and down-sampled the data to a coarser Ground Sample Distance (GSD), and Nurminen et al. (2013) compared different proportions of image overlap, but further research into acquisition specifications is still needed. Although these studies have demonstrated the potential of DAP to measure forest structure, variation in study configurations prevent the identification of optimal acquisition parameters for forestry applications.

In light of the imagery collected regularly over the conterminous USA for the NAIP program, the performance of pushbroom imagery is especially relevant today for large area forest inventory and mapping. However, there is a need to better understand the characteristics of both pushbroom and frame-based DAP with respect to unique features of these datasets, how they compare with lidar, and how effectively they can be used to predict forest attributes typically derived from field measurements. To assess these characteristics of DAP, we collected, processed, and analyzed temporally coincident lidar, frame-based DAP, pushbroom DAP, and field measurements. These coincident data enable direct comparisons between multiple remote sensing datasets with different acquisition specifications, and an evaluation of their explanatory power when modeling forest attributes.

The objectives of this study are to described key differences in properties of DAP datasets resulting from resolution and sensor differences, and to contrast the suitability of the different DAP datasets to model forest attributes in an Area Based Analysis (ABA; here we use ABA to describe the plot-level summarization of forest and remote sensing variables, which should not be confused with "Area-Based Approach" used in an estimation context). Although other studies have attempted to address some aspects of sensor differences, to our knowledge this is the first study that compares the potential of different resolutions of frame-based imagery, pushbroom imagery, and lidar collected in the same area to predict forest attributes. We first visually and statistically examine the point clouds from DAP and lidar and compare and contrast their properties with respect to canopy features and errors (such as gaps, individual trees, and canopy penetration). Next we evaluate differences in point cloud derivative metrics computed from each dataset, such as cover, coefficient of variation of heights, 5th percentile height, and 90th percentile height. We then perform a modeling analysis using two approaches. The first modeling approach is to identify the types of variables with the greatest predictive power and to assess the potential explanatory power of each dataset. The second approach relies on a fixed set of predictors to measure the relative explanatory power of respective datasets. Point cloud differences, calculated metrics, and model results are used to make inferences about the effects of resolution and sensor type, and the relative suitability of pushbroom and frame based DAP to model forest attributes. The findings from this study can be used to evaluate DAP as a tool for large-area forest inventory and modeling.

2. Methods

2.1. Study site

The study site is a 475 km^2, predominately low elevation (1–1007 m), forested area along the Hood Canal, east of the Olympic Mountains in western Washington, USA, centered on −122.96° longitude, 47.52 latitude (Fig. 1). The site is managed by the Washington State Department of Natural Resources for multiple uses including recreation, timber production, and wildlife habitat. The site is dominated by conifer species including Douglas fir (Pseudotsuga menziesii (Mirb.) Franco), western hemlock (Tsuga heterophylla (Raf.) Sarg.), and western redcedar (Thuja plicata Donn). There is a lesser presence of broadleaf trees including red alder (Alnus rubra Bong.) and bigleaf maple (Acer macrophyllum Pursh). Mature stands have high cover values (> 75%) in this area.

2.2. Field measurements

Field measurements were taken on 0.04 ha (0.1 acre) fixed area circular plots designed specifically for use with remote sensing data and included total tree height, diameter at breast height (DBH), species, age, and growth increment assessed with an increment borer. Tree volumes were computed by integration of whole tree taper equations (Flewelling, 1994). Plot locations were surveyed using Javad[1] Triumph 2 receivers. While no formal positional accuracy assessment was conducted for this study, according to the results from another study in similar conditions and in the same biome (McGaughey et al., 2017), we expect positional precision (horizontal RMSE) on the order of

[1] The use of trade or firm names in this publication is for reader information and does not imply endorsement by the U.S. Department of Agriculture of any product or service.

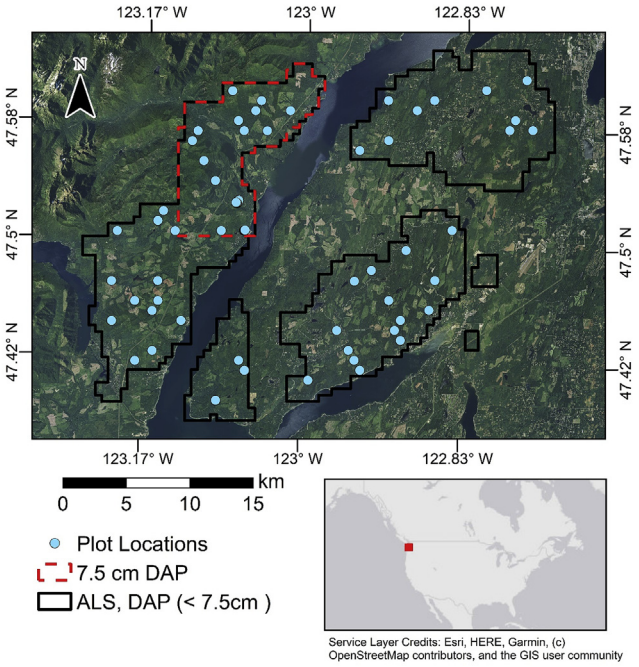

Fig. 1. Spatial distribution of remote sensing datasets and field plots. The extent of the 7.5 cm data is denoted in red.

Table 1
Summary of field measurement derived forest attributes with lidar P90 and Cover for 57 plots.

Statistic	ba	volume	Lorey's Ht	trees/ha	lidar P90[a]	lidar Cover[a]
Min	0.4	0	1.4	0	0.3	0.5
25th Pct	21.9	141.4	15.3	247.6	14.8	73.9
Median	34.1	351.6	24.3	371.4	25.6	95.2
Mean	36.2	354.4	22.7	383.6	22.4	79.5
75th Pct	47.2	527.8	29.7	544.7	30.5	98.8
Max	104.7	1022.2	43.2	916.1	47.8	99.9

*basal area is abbreviated as "ba".
[a] P90 and Cover are defined in Table 3.

approximately 1 m. Field measurements were taken during the spring of 2015. A total of 61 plots were measured, of which 6 were not used because they were harvested in the few months between field measurements and the remote sensing campaigns. Field measurement derived forest attributes and two remote sensing attributes are summarized for field plots in Table 1.

2.3. Remote sensing data

Frame camera imagery and pushbroom sensor data were processed to create 3D point clouds using photogrammetric software. The process uses overlapping views of the same area acquired from different viewpoints to build 3D models. In the case of frame cameras, a large rectangular sensor array captures overlapping frames (images) along the aircraft flightline (Fig. 2, Frame Camera). The amount of overlap is planned in advance considering the flying height, aircraft speed, camera field-of-view, and time (distance) between frames. Additional overlap is provided by side-to-side overlap between adjacent flightlines (not shown). Airborne pushbroom sensors, in contrast, use multiple sensor arrays angled forward, nadir, and backwards which scan continuously along the flight path (Fig. 2, Pushbroom Sensor). For a given view angle, the sensor array used to collect pushbroom data consists of thousands of pixels in the across-track direction, but only a single pixel in the along-track direction. Overlap is created from the scans using the intersection of different view angles. For example, the area on the ground scanned by the nadir sensor is scanned a short time later by the rear facing sensor. These two different view angles for the same location provide the stereo overlap required for photogrammetric processes.

Table 3
Description of a subset of point metrics provided by FUSION software.

Metric	Description[a]
P05	5th percentile height above 2 m
P30	30th percentile height above 2 m
P80	80th percentile height above 2 m
P95	95th percentile height above 2 m
CV	Coefficient of variation of heights above 2 m
Min	Minimum height above 2 m
Cover	proportion of heights above 2 m
MN2	generalized mean for squared heights
MN3	generalized mean for cubed heights
CRR	canopy relief ratio

[a] as defined in the FUSION documentation.

The frame camera imagery were collected at 7.5 cm, 15 cm, and 30 cm nominal GSDs by GeoTerra Inc. in the late spring of 2015 (see also Table 2 for a summary of acquisition specifications) using the Vexcel Imaging UltraCamXP with a focal length of 100.5 mm and a pixel size of 6.0μm × 6.0 μm. Imagery was flown with 60% endlap and 30% sidelap. Frame camera imagery were processed using the Trimble Inpho software (Trimble Inpho, 2019). Aerial triangulation was performed in a semi-automated way, where tie points were generated using point matching techniques, and then reviewed to ensure quality. Aerial triangulation for the three sets of imagery used airborne GNSS, photo centers, and 16 survey control coordinates.

Pushbroom imagery were collected "leaf-on" for all of Washington State in 2015 by North West Geomatics Ltd. with a Leica ADS100 SH100 sensor. The ADS100 sensor has three view angles, 25.6° forward, nadir, and 19.4° back. Only the nadir and rear view angles were used for point cloud creation. The imagery were collected from an average flying height of 5000 m resulting in a 40 cm nominal pixel GSD. The images were processed with the BAE Socet GXP Auto Spatial Modeler (ASM) module (Walker and Pietrzak, 2015). A highly customized configuration file including nearly 100 settings was used with BAE Socet GXP to process the pushbroom imagery into a point cloud suitable for forestry purposes. The 40 cm pushbroom imagery is henceforth referred to as "40 cm PB".

Table 2
Summary of acquisition parameters for remote sensing datasets.

								RMSE (meters)		
Sens. type	Mfr.	Model	F. lap	S. lap	Res.	Acq. Date	Area (km^2)	x	y	z
Frame	Vexcel	UltraCamXP	60%	30%	7.5 cm	Spring 2015	88	0.06	0.06	0.06
Frame	Vexcel	UltraCamXP	60%	30%	15 cm	Spring 2015	475	0.05	0.05	0.11
Frame	Vexcel	UltraCamXP	60%	30%	30 cm	Spring 2015	475	0.15	0.15	0.15
Pushbroom	Leica	ADS100	100%	10%	40 cm	Summer 2015	475	–	–	–
Lidar	Optech	Orion	–	50%	8 ppm	Winter 2015	475	–	–	0.05

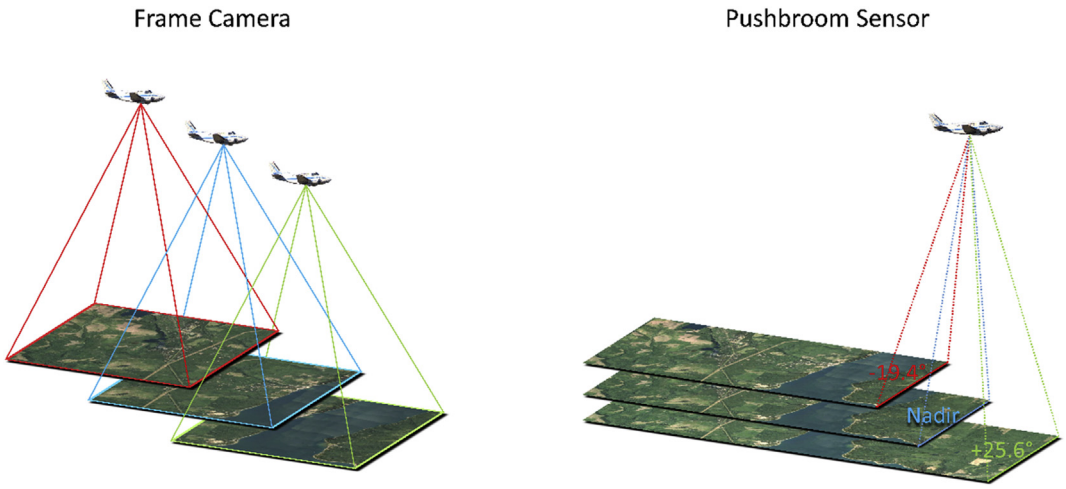

Fig. 2. Stylized depictions of the area covered by frame-cameras and pushbroom sensors. The view angles for the pushbroom sensor are specific to the Leica ADS100 SH100 sensor used in this study.

Lidar data were collected in mid-February of 2015 by GeoTerra Inc. at a nominal density of 8 emitted pulses per square meter (ppm) using an Optech Orion H300 system mounted on a fixed-wing aircraft. The data were collected with a 200 kHz pulse repetition frequency and scan rate of 66 scan lines per second. The target flying height was 1200 m above ground level, and a target ground speed of 176 km/h. The minimum overlap between lidar strips was 50% with a +-15° field of view. Lidar data were processed in Optech's Lidar Mapping Suite. Aircraft trajectories were calculated by combining IMU data with differentially corrected onboard GNSS data. After a relative solution was created to combine points from all lidar strips, 15 ground control points were used to adjust the solution to the local coordinate system. The Optech Orion H300 records up to 4 range measurements per laser pulse emitted. Only first returns were used in this study. The vendor classified ground returns from lidar using the Optech Lidar Mapping Suite. The points were then used to generate a triangular irregular network that was then rasterized to produce a 1 m Digital Terrain Model (DTM).

2.4. Point cloud processing

Processing of each of the remote sensing point clouds was performed using with the US Forest Service FUSION software (McGaughey, 2016). Aside from visual examinations, point data were used as summaries or "metrics" computed at the plot or pixel level. The metrics are statistics (e.g. percentiles, standard deviation, mean, kurtosis, skewness, height ratios) computed from point heights relative to the lidar digital terrain model (DTM). Point heights were computed as the difference between point elevations and lidar DTM. Lidar metrics were computed using only the first returns.

The "GridMetrics" and "CloudMetrics" tools within FUSION were used to generate wall-to-wall raster layers of height metrics at 20 m resolution and at the plot level respectively. GridMetrics and CloudMetrics provide on the order of 100 different metrics computed for point data. The metrics used in this study are described in Table 3.

2.5. Model fitting and variable selection

Models were fit between field-measurement derived forest attributes and point cloud metrics using Ordinary Least Squares (OLS) regression using the R statistical environment (R. Core Team, 2018). The large number of available predictor variables necessitated a formalized approach to variable selection. Two approaches were used for variable selection including automated variable selection, and expert model selection. In automated variable selection an algorithm was used to choose an optimal set of predictors. In expert model selection, the expert defines a single or "fixed" model structure for all datasets which accurately describes the response, is resistant to outliers, and accounts for auxiliary variable collinearity. The simple application of these approaches in this study is designed only for transparent assessment of the properties of the different datasets while minimizing confounding influences. In practice, models fit for the purpose of area-wide predictions typically involve many iterations of variable selection, diagnostics, and expert interaction, which can confound inferences about inherent differences between datasets.

The Leaps and Bounds algorithm (Furnival and Wilson, 1974; Thomas Lumley, 2017) was used for automated variable selection. This was to distinguish differences in the types of point cloud metrics which are suited to modeling forest attributes for the various remote sensing datasets. An example metric which behaves differently between Lidar and DAP is P05. Calculated from lidar data, it provides little or no explanatory information for field measurement based forest attributes. This is because P05 values from lidar tend to fall very close to the minimum height, typically the minimum height used to filter near-ground vegetation. P05 from DAP, on the other hand, tends to be higher in the canopy because DAP points do not penetrate dense canopy like lidar does. While automated variable selection works well for data exploration, it is problematic to rely on exclusively because it can result in spurious correlation and in fitting of models to artifacts in the data instead of to actual physical relationships. This approach often leads to poor prediction performances for models that appear to have superior explanatory power. Ranking the explanatory power of datasets following automated variable selection is also problematic because the automated selection process introduces randomness, especially for small samples.

For the expert or fixed modeling approach a single model form and set of predictors was applied for each dataset and forest attribute. This fixed modeling approach provides a measure of the relative explanatory power of each dataset when the model form is held constant. A fixed model also provides increased model stability relative to automated variable selection; there is reduced risk of overfitting the data when a fixed set of predictors is used. However, care should be taken that the set of predictors is appropriate for all of the datasets (e.g. a model including P05 would not be appropriate because P05 behaves differently for DAP and lidar). Finding models which explain the most variation is not the objective of this approach. The objective is to rank datasets by the amount of variation explained when the choice of variable is held constant.

The fixed set of predictors that we used to model all forest attributes included P80, cover, and the interaction between P80 and cover:

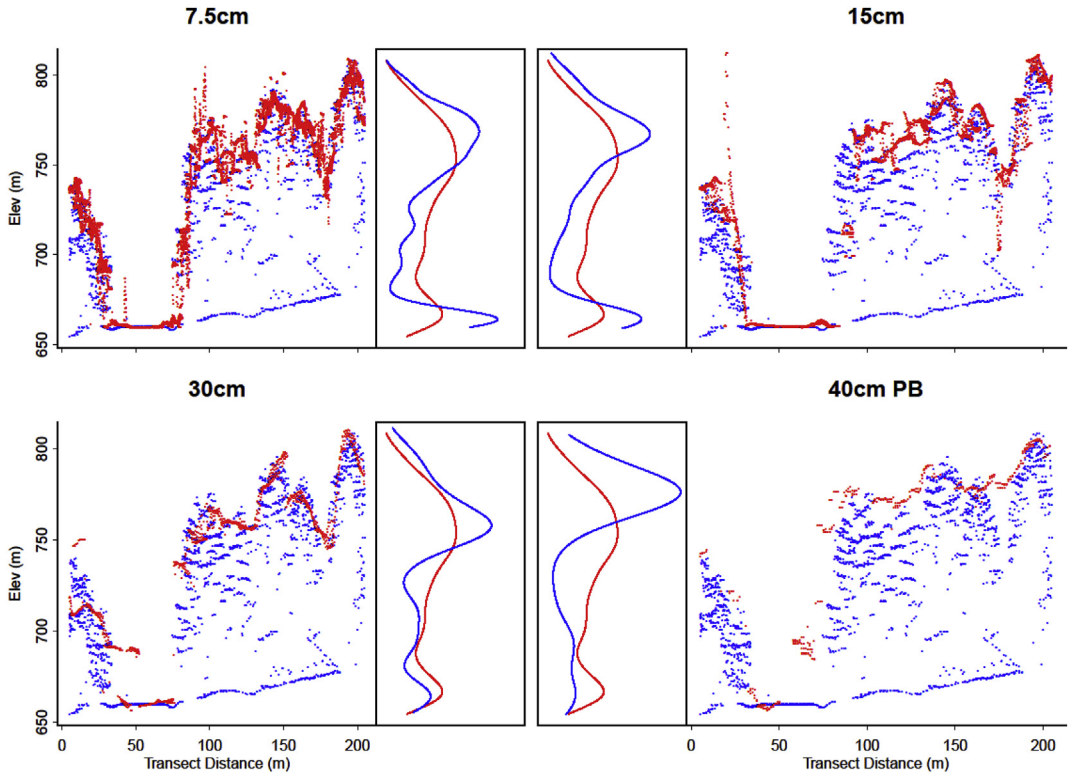

Fig. 3. Comparisons of vertical point densities and point cloud scatter plots for DAP (blue) and lidar (red). The densities represent the relative proportion of observations for a given elevation.

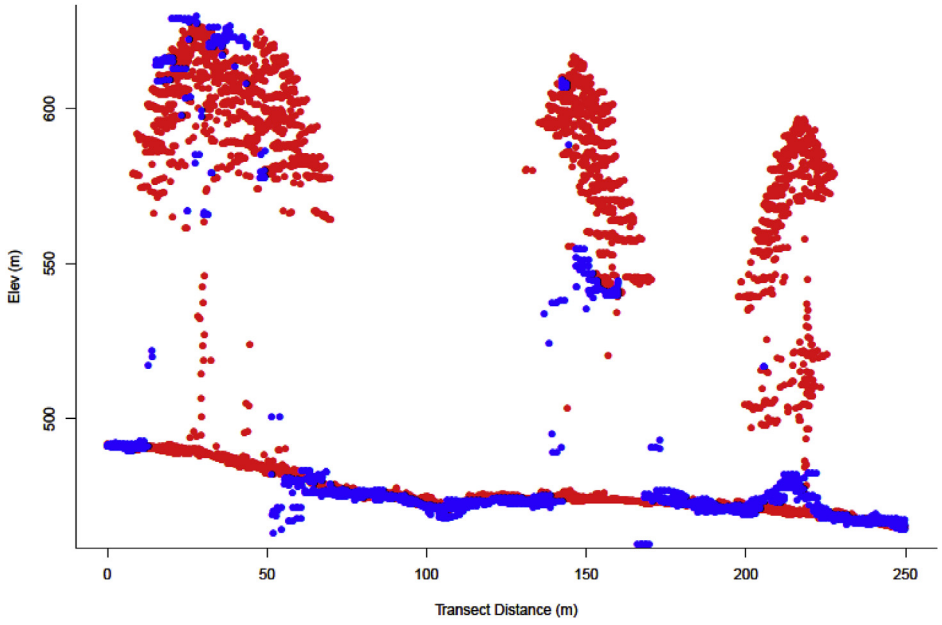

Fig. 4. Example showing different levels of omission of individual trees by 40 cm pushbroom DAP (blue) relative to lidar (red).

$$y = \hat{\alpha} + \hat{\beta}_1 P80 + \hat{\beta}_2 Cover + \hat{\beta}_3 (Cover \times P80) + \hat{\varepsilon}. \quad (1)$$

y is a vector of field measured forest attributes
$\hat{\alpha}$, $\hat{\beta}_i$ *are estimated model coefficients*
$\hat{\varepsilon}$ *is a vector of residual errors*
P80 and cover are remote sensing metrics as defined in Table 1.

3. Results

3.1. Point cloud comparisons

Fig. 3 provides 3D slices of the point clouds for identical locations in each of the datasets. In Fig. 3, results for the 7.5 cm imagery contained a large number of errors. Despite re-processing the 7.5 cm data a number of times with different configurations, the DAP software frequently produced errors when matching targets in the forest canopy. We also

attempted to process the 7.5 cm data in VSfM (Furukawa and Ponce, 2010; Wu, 2013), SURE (Rothermel et al., 2012), and Agisoft Photoscan (Agisoft Photoscan Professional Edition, 2019) and observed the same types of errors (results not shown). For frame-based imagery, coarser resolution imagery provided less structural detail, but also had fewer obvious errors. The errors appear to be the result of a combination of the acquisition resolution, relatively low image overlap (60% forward lap, 30% side lap), and the structural complexity of the forested environment. The densities in Fig. 3 indicate that the distributions of DAP points are generally skewed towards the canopy surface relative to the distribution of lidar points. In Fig. 3 there is a density spike in both lidar and DAP datasets near the ground; for DAP the spike is the result of the canopy gap and would not be present for DAP in a closed canopy example.

Common DAP errors include pits, gaps, spikes, interpolated crown edges, general over-smoothing, poor horizontal alignment, and individual tree omissions. Fig. 3 demonstrates some of these common errors including spikes (7.5 cm and 15 cm), over-smoothing (30 cm and especially 40 cm PB), and poor horizontal alignment (30 cm and 40 cm PB). In Fig. 4 we see an example of omission of individual trees in an opening by DAP. DAP algorithms either remove these points as errors, or the search windows for tie points on the ground do not reach the tree crowns.

Fig. 5 shows examples of the agreement between metrics for 20 m cells computed from DAP heights versus those computed from lidar first return heights and summarizes their relationships. Table 4 quantifies the linear agreement between lidar and DAP height metrics with R^2 for a greater number of combinations of metrics and data sources. As we can see in Fig. 5, there is a strong linear relationship between cover computed from DAP and from lidar: the relationship corresponds to R^2 values ranging from 83% to 91% in Table 4. For cover computed from frame-based DAP, there is a very slight trend for R^2 values to decline with reduced resolution, with a much larger drop in R^2 (5%) occurring for 40 cm pushbroom data. For frame-based DAP, the decline in R^2 cover as a function of resolution is practically insignificant for ABA for the resolutions examined here.

In Table 4, the agreement between DAP and lidar height percentiles is generally greatest for the upper canopy height percentiles P80 and P95. R^2 values for P80 and P95 were generally very similar for a given data source, and ranged from 71 to 82%. Based on the visible agreement between P80 values from DAP and lidar in Fig. 5, it would be reasonable to expect that upper canopy height percentiles would have greater R^2 values than cover because the spread of values around the 1-1 line appears much tighter for P80 than for cover. However, there is a cluster of outlier points beneath the 1-1 line, where lidar heights are consistently greater than DAP heights. An examination of these pixels found that the outliers were typically in areas with a few scattered trees, where the DAP software failed to detect the individual trees, but the trees were present in the lidar. Unlike cover, the agreement between lidar and DAP upper canopy height percentiles appears to increase for coarser image resolutions, except for the 40 cm pushbroom data which had poorer agreement with lidar than the 30 cm data. The poorer agreement for the 40 cm data was likely due to the fact that the 40 cm data were collected with a pushbroom sensor rather than due to any resolution effects.

The agreement between lidar and DAP for lower canopy height percentiles declined relative to upper canopy height percentiles: there was 1–8% decline in R^2 values for P30, and a more dramatic 13–30% decline for P05. The results for P05 in Table 4 and Fig. 5 are consistent with our expectations for lower canopy metrics, given that DAP points are less likely to exist below the upper canopy for areas with dense upper canopies. This phenomenon can be seen in the cluster of points above the 1-1 line in Fig. 5, which indicates that there is a positive bias in DAP derived P05 relative to lidar derived P05. The low R^2 for P05 in Table 4 isn't necessarily a negative implication for using DAP in ABA, it simply indicates that P05 provides a different kind of information about forest structure when it is computed from DAP compared to when it is computed from lidar. This is different than the bias observed for P80 determined to be the result of errors in the detection of individual trees by the DAP software.

We can see how the relationships between lidar and DAP height metrics translate to mapped outputs in Fig. 6. The differences between lidar and DAP (shown for 30 cm and 40 cm pushbroom DAP) for cover and P80 are highly spatially clustered in harvested areas. Clustered negative differences (red; DAP greater than lidar) tend to reflect individual trees in otherwise open areas that were not detected by DAP, and clustered positive values (blue; lidar greater than DAP) tend to reflect management activities that occurred at a time after the lidar data were collected and before the imagery were collected (lidar was collected in the late winter, and imagery in the late spring). Differences in P05 and Cover are predominately negative, while the distribution of differences in P80 is more symmetric around zero. The spatial pattern of P05 differences are concentrated in areas with the tallest trees (height map not provided). This follows from what we can see in Fig. 5 and Table 4, that DAP tends to measure P05 higher than lidar. We also see agreement between Fig. 6 and Table 4 that there are fewer extreme differences between lidar and DAP in the 30 cm imagery than in the 40 cm pushbroom imagery for all height metrics. This can be also be seen from the densities in that the tails are thicker for 40 cm pushbroom than for 30 cm imagery.

In Table 5, the correlations between prominent auxiliary variables are shown to vary by dataset. All of the datasets show similar levels of correlations between P30, P80, P95, and Cover with 40CM PB having the highest correlations amongst these attributes, and the smallest in magnitude correlations with CV. The difference in behavior for CV from 40CM PB is due to the fact that the 40CM PB canopy surface tends to be relatively smooth, regardless of canopy height, while the other datasets have increased surface variation with increased canopy height. With the exception of CV for 40CM PB, DAP datasets in general show slightly higher magnitude R^2 values amongst all auxiliary variables than the lidar auxiliary variables, suggesting that they contain less independent information about forest structure than is present in the lidar. P05 for lidar has a very low correlation with other auxiliary variables due to the fact that it typically falls very near to the minimum height threshold.

3.2. Relationships between forest attributes and remotely sensed forest structure

Fig. 7 shows examples of scatterplots showing the relationships between remotely sensed heights (P90) and forest attributes. The lidar and 30 cm data in Fig. 7 have quite similar patterns and their spreads do not vary greatly. Trees per ha appears to have a poor and perhaps non-linear relationship with remotely sensed height, whereas Lorey's height has a strong linear relationship. While we do not provide scatterplots for the remaining remote sensing datasets, the relationships they depict are similar to the cases shown in Fig. 7.

Table 6 shows the R^2 values that were achieved by OLS with automated variable selection. Due to the small number of observation and the limited data extent, the 7.5 cm dataset cannot be easily compared with the other datasets, especially since we used automated variable selection for this result. The risk of overfitting with variable selection is especially problematic for 7.5 cm data due to only having 20 observations. For this reason we provide the 7.5 cm results for demonstrative purposes, but concentrate our inferences on the remaining datasets.

Lidar generally performed better than other datasets with respect to both R^2 and RMSE, although results for 15 cm and 30 cm datasets were generally similar to lidar. The exception is trees/ha, for which lidar explained at least 12% more variation than other datasets, and its RMSE was 8% smaller (better). The 40 cm pushbroom dataset fared the worst in each case, explaining 1%–4% less variation than the next poorest performing dataset in each case and about 2% higher RMSE values. The analysis did not provide strong evidence that resolution played a

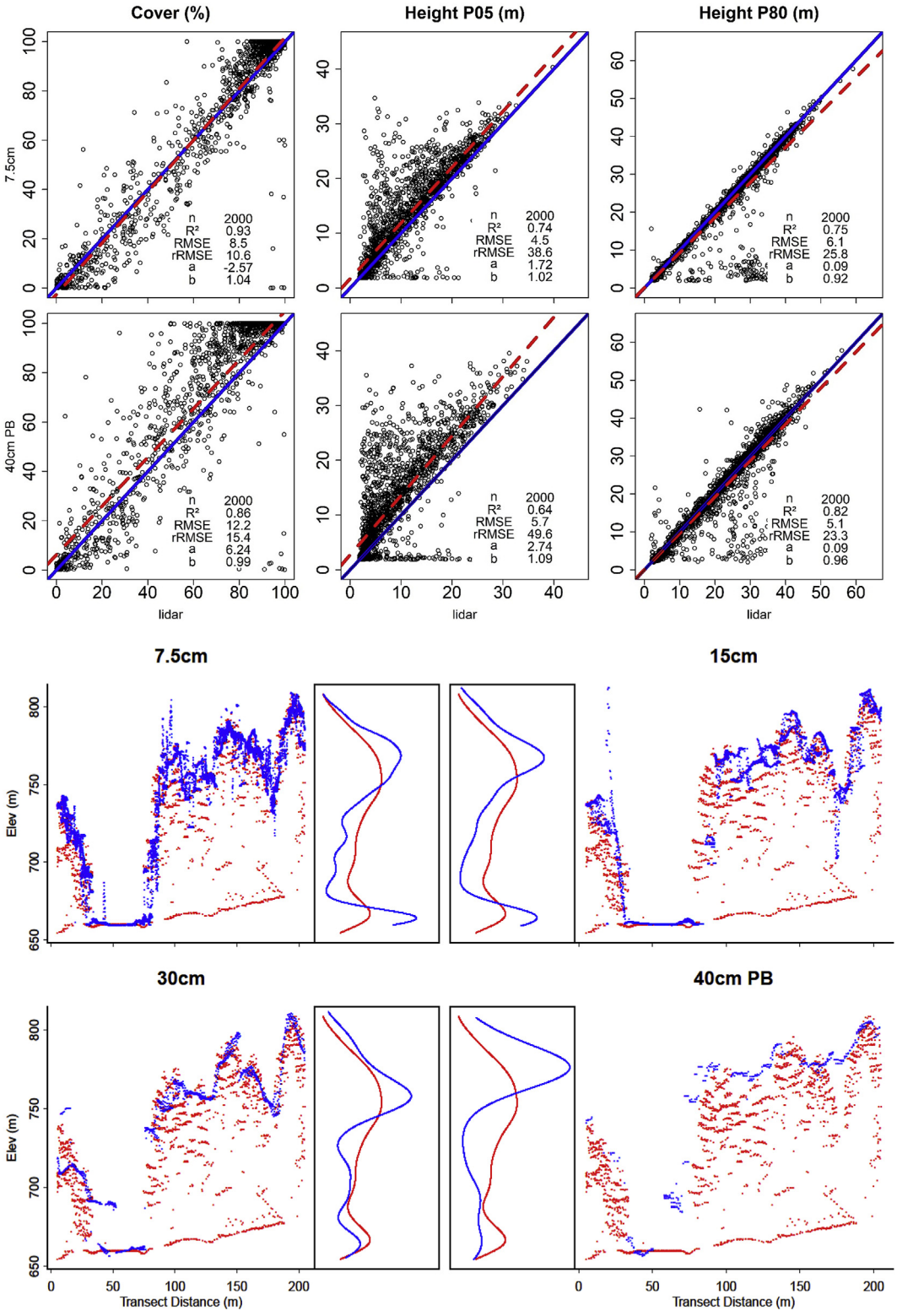

Fig. 5. Scatterplots between 7.5 cm (frame) and 40 cm pushbroom (PB) DAP height metrics (Y axes) relative to lidar height metrics (X axes) computed for a sample of 2000 20 m cells. Blue lines represent 1-1 lines, and red lines represent linear models fit between DAP and lidar metrics. Model summaries are provided in the lower right corner including the number of pixels sampled (n), the coefficient of determination (R^2), RMSE, relative RMSE (rRMSE, in percent), intercept (a), and slope (b).

practically significant role in performance. For example, the 15 cm data performed worse than the 30 cm data on average, despite theoretically holding four times as much information.

The highest resolution dataset, 7.5 cm, generally fared as well as or slightly better than other DAP datasets, but as previously mentioned, there is a high chance that the models over-fit the 7.5 cm data. It is also likely that the distribution of forest attributes measured by the 7.5 cm data is fundamentally different from the remaining datasets. This is evident from the similar R^2 values observed amongst all datasets for trees/ha, but the much smaller RMSE value observed for 7.5 cm data.

Table 4
Coefficients of determination (R^2) between DAP datasets and lidar for the same metrics for a sample of 5000 pixels.

	DAP Datasets			
Metric	7.5 cm	15 cm	30 cm	40 cm PB
Cover	90.56	89.95	88.39	83.4[a]
CV	44.64	45.49	45.43	39.06
Min	2.89	0.17	0.15	0.19
P05	55.51	47.35	50.84	48.06
P30	68.89	71.59	80.11	74.18
P80	71.13	79.2	81.35	76.36
P95	74.29	78.88	81.59	75.7

[a] R^2 values in Table 4 and Fig. 5 differ because the values were calculated for samples.

The results in Table 7 suggest that there are some differences in the automated variable selection results from each of the remote sensing datasets. P05 is commonly pulled into 7.5 cm models and once each for 15 cm and 30 cm datasets, but is not used in any of the lidar models. Another feature of 7.5 cm models is that only height percentiles were selected by the Leaps and Bounds algorithm, while models for other datasets included a variety of predictor types. There are also similarities amongst datasets; for example in the 7.5 cm and lidar models there are commonly low and high height percentiles in the same model. A metric which has rarely been used by other studies, but was found in 15 cm, 30 cm, and 40 cm pushbroom models was the generalized mean squared height (MN2). The model for trees/ha was consistent in using a 3 variable model, except for the 7.5 cm dataset where we only allowed 2 predictors to enter the model. Cover and upper canopy percentile (P99 or P95) were common predictors used for trees/ha by the various datasets.

Results from the model fitting process with a fixed set of predictors can be seen in Table 8. The variation explained by the fixed models was

Table 5
Coefficients of determination (R^2) between remote sensing auxiliary variables.

data	metric	P05	P30	P80	P95	Cover	CV
7.5 cm	P05	1	0.79	0.58	0.55	0.28	0.31
7.5 cm	P30		1	0.83	0.77	0.51	0.5
7.5 cm	P80			1	0.97	0.57	0.62
7.5 cm	P95				1	0.52	0.54
7.5 cm	Cover					1	0.95
7.5 cm	CV						1
15 cm	P05	1	0.9	0.73	0.66	0.61	−0.2
15 cm	P30		1	0.89	0.81	0.76	−0.25
15 cm	P80			1	0.98	0.78	−0.29
15 cm	P95				1	0.74	−0.29
15 cm	Cover					1	−0.39
15 cm	CV						1
30 cm	P05	1	0.84	0.53	0.45	0.37	0.08
30 cm	P30		1	0.69	0.6	0.54	0.11
30 cm	P80			1	0.95	0.55	0.12
30 cm	P95				1	0.54	0.11
30 cm	Cover					1	0.22
30 cm	CV						1
40CM PB	P05	1	0.9	0.67	0.63	0.42	0
40CM PB	P30		1	0.84	0.79	0.55	0
40CM PB	P80			1	0.98	0.57	0
40CM PB	P95				1	0.57	0
40CM PB	Cover					1	0.01
40CM PB	CV						1
lidar	P05	1	0.1	0.03	0.02	0.19	0.11
lidar	P30		1	0.55	0.42	0.42	0.3
lidar	P80			1	0.95	0.51	0.37
lidar	P95				1	0.46	0.31
lidar	Cover					1	0.7
lidar	CV						1

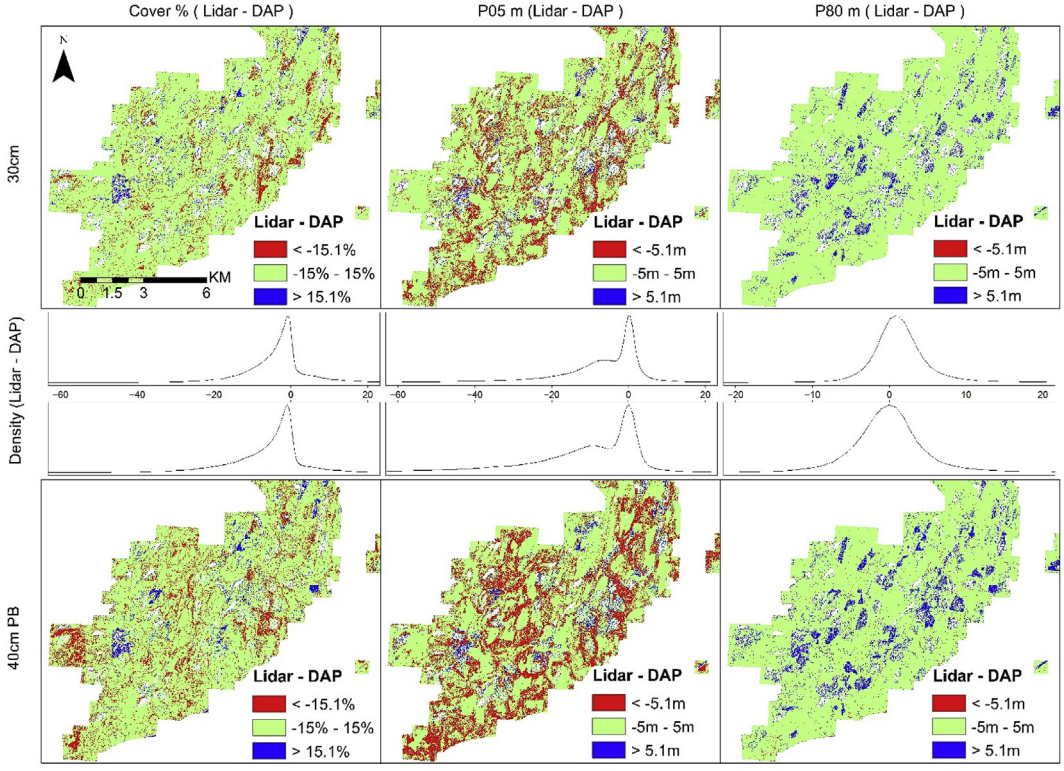

Fig. 6. Mapped differences and densities of differences between lidar and DAP height metrics for 30 cm and 40 cm pushbroom data. The X axes for the densities are in percent for cover and meters for P05 and P80.

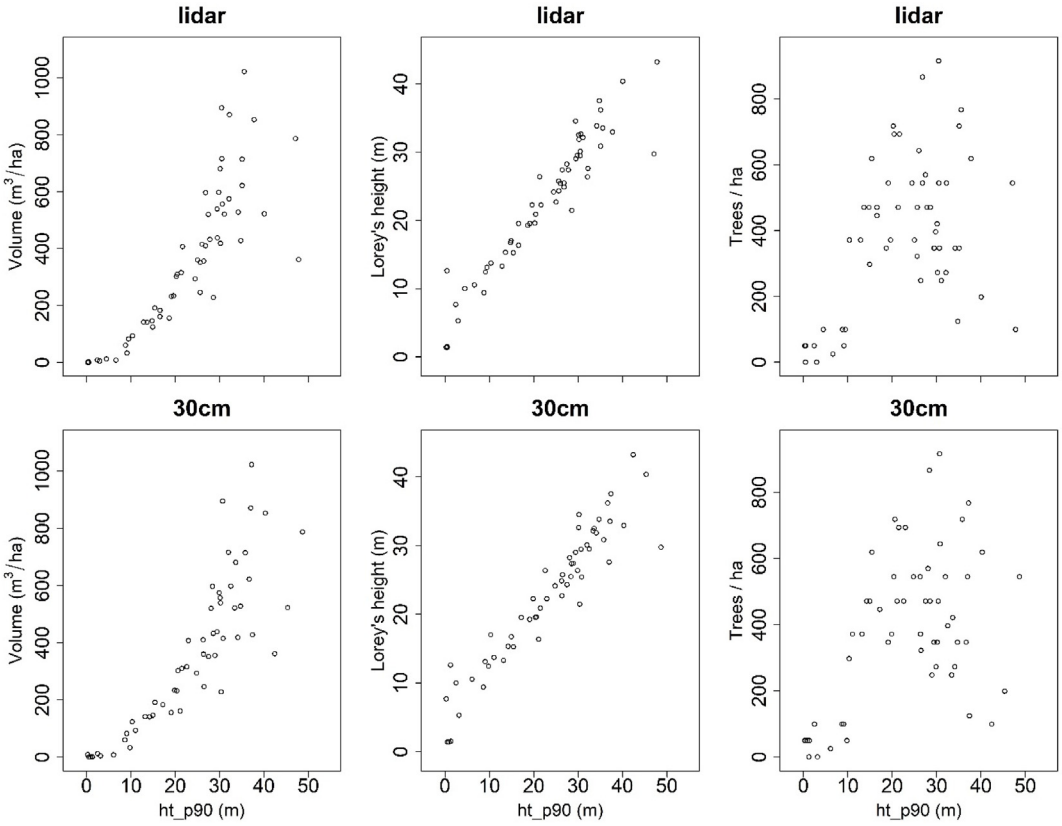

Fig. 7. Scatterplots showing the relationships between field measurement based forest attributes (volume, Lorey's height, trees/ha) and remotely sensed heights (ht_p90) for lidar and 30 cm DAP.

Table 6
R^2 and RMSE values in percent for *automated variable selection* models fit between forest attributes and remote sensing attributes.

		ba		volume		Lorey's ht		trees/ha	
dataset	n	R^2	RMSE	R^2	RMSE	R^2	RMSE	R^2	RMSE
7.5 cm[a]	20	79	22	88	20	90	10	57	30
15 cm	57	71	38	83	32	91	13	55	42
30 cm	57	75	35	82	32	91	13	58	40
40 cm PB	57	67	40	78	35	89	15	50	44
lidar	57	73	37	85	30	91	13	70	34

[a] 7.5 cm data should not be compared directly with other datasets due to the limited number of plots available for use with 7.5 cm data.

generally less than what was explained by automated model selection shown in Table 6 and had higher RMSEs. The results also generally agree with the results for automated model selection in that lidar explained more variation than other datasets and had lower RMSE values. When excluding the 7.5 cm data, differences in the proportions of variation explained between automated model selection and fixed models for ba, volume, and Lorey's height were slight, ranging from −5 to 3 percent. The differences in explained variation for trees per ha were much greater for all of the datasets, ranging from −18 to −22 percent (excluding 7.5 cm data). This would suggest that the predictors in the fixed models are poorly suited for trees per ha. Despite this we see a pattern for trees per ha consistent with other attributes: resolution has a minimal effect, 40 cm Pushbroom DAP performed the worst, and lidar performed the best. The differences between automated model selection and fixed models were most dramatic for the 7.5 cm dataset; the 7.5 cm dataset saw a 10 to 58 percent decline in R^2 relative to using automated model selection, likely due to over-fitting with automated model selection.

4. Discussion

4.1. DAP versus lidar

DAP and lidar are fundamentally different technologies which can both measure aspects of vertical forest structure. While data from both technologies can be stored as point clouds and used similarly for forest inventory, there are distinct differences in the components of vertical forest structure they measure. As we saw in the point clouds in section 3.1 (Fig. 3), lidar has information about vertical structure throughout the canopy. DAP, in contrast, only measures elevations along the surface of the canopy. To obtain canopy height measurements from DAP (versus elevations), we required a DTM from another source. Height metrics can be computed for both DAP and lidar point clouds, although depending upon the metrics and forest conditions, computed values may be very similar or quite different for the same pixel location.

Upper canopy height percentiles from DAP and lidar were found to have a very strong linear relationship both visually and statistically, except in areas with sparsely distributed trees where the DAP software failed to produce data points representing the lone trees. This problem was evident regardless of resolution and sensor type. In contrast to our expectations, there was also a strong linear relationship between DAP and lidar derived cover metrics. The fact that DAP cover values varied along with lidar cover values suggests that canopy gaps, openings, and edges – conditions where DAP points do occur near the ground – play a large role in the distribution of cover values, even when forest conditions are predominately closed-canopy.

The scatterplots for P05 in Fig. 5 and the automated variable selection exercise with variables listed in Table 7 demonstrate that the same metric computed for lidar and DAP are not necessarily measuring the same thing. P05 especially was shown to provide usable information about canopy structure when derived from DAP, but when derived from

Table 7
Variable selection results for combinations of remote sensing datasets and forest attributes.

Dataset	Forest Attr.	X1	X2	X3
7.5 cm	volume	P05	P99	
7.5 cm	ba	P05	P80	
7.5 cm	trees/ha	P80	P95	
7.5 cm	Lorey's ht	P70	P99	
15 cm	volume	MN2	Cover	
15 cm	ba	MN2		
15 cm	trees/ha	P95	MN3	Cover
15 cm	Lorey's ht	P99		
30 cm	volume	MN2		
30 cm	ba	P05	P10	P50
30 cm	trees/ha	P60	P99	Cover
30 cm	Lorey's ht	P95		
40 cm PB	volume	MN2		
40 cm PB	ba	MN2		
40 cm PB	trees/ha	P60	P95	Cover
40 cm PB	Lorey's ht	P80		
lidar	volume	P30	P75	CRR
lidar	ba	P40	MN3	
lidar	trees/ha	P80	P99	CRR
lidar	Lorey's ht	P20	P90	

lidar it was too closely related to the canopy threshold (2 m) to be of use. As demonstrated by P05, the degree of association between DAP and lidar metrics does not necessarily mean that DAP metrics are inferior to the equivalent lidar metrics. However, our results do suggest that DAP height metrics were generally able to explain less variation in volume, basal area, Lorey's height, and trees per ha than lidar metrics, regardless of the DAP sensor type or resolution. This was the case for both fixed models and model developed with automated variable selection (where the 7.5 cm data was excluded from consideration). There may, however, be opportunities for further improvements to DAP performance by using metrics better suited to the strengths of DAP that are either not available or not typically computed for lidar data. Examples include metrics from RGBI values (Kukkonen et al., 2019) and voxel based metrics (Kim et al., 2016).

There is one major practical difference between lidar and DAP. Lidar can be used to create DTMs because it penetrates through small opening in dense canopies to measure the ground. DAP typically does not provide data representing the ground under canopy thus it can only be used to produce DTMs in open, non-vegetated areas. The fact that DAP cannot be used to create DTMs in densely vegetated areas means that, as previously mentioned, another source of DTM must be paired with DAP to be able to measure canopy height information with DAP. While lidar is arguably the best source of mapped elevation data, there are large proportions of the western half of the USA which do not have publicly available lidar. In an ideal scenario, lidar is collected for the first iteration of forest yield modeling which can be used to acquire a DTM. Subsequent updates could then be implemented with DAP in combination with lidar DTMs. An alternative is to use coarser resolution datasets that are often available at the national level, such as the National Elevation Dataset (NED) for the USA. Studies have found that a 10 m DTM can be used with DAP for forestry applications (Kukkonen et al., 2017; Strunk et al., 2019), although there is evidence of a reduction in performance relative to using DAP with a lidar DTM.

4.2. Pushbroom versus frame-based DAP

Because the frame camera and pushbroom sensor resolutions differed, our findings with respect to sensor are not definitive, but they are highly suggestive that the pushbroom sensor DAP performed slightly worse than the frame camera DAP. Effects of using a pushbroom camera instead of a frame camera were evident both in the profiles of canopy heights, and in the results for ABA. Pushbroom DAP had much less fine-scale canopy detail than the other datasets, and there was an approximately 10% penalty with respect to ABA model performances. While the resolution of pushbroom DAP was 10 cm coarser than the any of the frame camera datasets (40 cm versus 30 cm), the lack of a resolution effect observed between 15 cm and 30 cm frame camera imagery would suggest that the different sensor type explained the performance reduction, not the 10 cm resolution difference.

4.3. Effects of DAP resolution

The highest resolution DAP dataset, 7.5 cm frame-based imagery, visually contained the greatest detail about the canopy surface. Unfortunately, there was also an increase in the number of errors in the 7.5 cm data, especially spikes. The number of errors decreased if we resampled the 7.5 cm imagery to coarser resolutions (results not shown), although this same result could be achieved more cost-effectively by simply acquiring coarser resolution imagery. In addition, the imagery collected at 15 cm resolution appeared to have a similar level of canopy detail as the 7.5 cm data, but contained fewer obvious errors. Results with the 7.5 cm imagery from other photogrammetric software also resulted in numerous errors (results not shown) indicating that our findings were not software specific.

While there were obvious visual differences in detail and presence of errors as a function of resolution, there appear to be minimal impacts on ABA from DAP resolution. Height metrics for the finest and coarsest resolution DAP datasets were similarly correlated with lidar height metrics. They also had similar relationships with field attributes, with a slight reduction in R^2 for the 40 cm pushbroom DAP – although as previously described, this was likely due to sensor differences rather than the 10 cm change in resolution. The finding that ABA was insensitive to resolution is of practical importance because it indicates that 30 cm DAP (and likely coarser resolutions) is suitable for ABA, reducing the costs associated with data collection and processing. The cost of a new 30 cm frame camera imagery collection for a project of

Table 8
R^2 and RMSE values in percent for *fixed* models fit between field measurement derived forest attributes and remote sensing attributes as well as change (Δ%) in R^2 relative to automated variable selection.

		ba		volume		Lorey's Ht		trees/ha	
dataset	n	R^2 (Δ%)	RMSE	R^2 (Δ%)	RMSE	R^2 (Δ%)	RMSE	R^2 (Δ%)	RMSE
7.5 cm[a]	20	71 (−11)	28	79 (−10)	27	50 (−44)	23	24 (−58)	41
15 cm	57	69 (−2)	39	80 (−3)	34	87 (−4)	16	45 (−18)	46
30 cm	57	71 (−5)	38	81 (−1)	34	86 (−5)	17	44 (−25)	46
40 cm PB[b]	57	63 (−5)	43	75 (−5)	39	89 (0)	15	40 (−20)	48
lidar	57	75 (3)	36	84 (−1)	31	89 (−3)	15	55 (−22)	42

[a] 7.5 cm data should not be compared directly with other datasets due to the limited number of plots availed for use with 7.5 cm data.
[b] 40 cm data were derived from a pushbroom (PB) sensor, while the other DAP resolutions were derived from a frame camera.

this size can cost from 1/3 to as little as 1/10th the cost of 8 ppm lidar for the same area including processing costs. The 7.5 cm imagery, in contrast, can cost as much or more than lidar for the same area.

4.4. Performances relative to other studies

Our findings agree with a number of prior studies in observing that DAP performs slightly poorer than lidar in explaining variation in forest attributes (e.g. (Järnstedt et al., 2012; Nurminen et al., 2013; Pearse et al., 2018; Vastaranta et al., 2013; White et al., 2015)). However, given the low price of DAP relative to lidar, most studies consider DAP to be a highly effective tool for measuring and re-measuring forest height. This is especially the case where the low cost of DAP makes forest inventory with remotely sensed structure viable, where it otherwise may not be viable due to the high cost of lidar. Another common scenario in which a DAP point cloud can prove even more affordable, is when there are already plans to acquire imagery for orthophotos, and the cost of additional processing to create a point cloud is minimal. The NAIP program is a good example of this, where the program collects stereo pushbroom imagery wall-to-wall over the entire conterminous USA on a regular basis and the cost to produce a point cloud from these data is small. Processing data from the NAIP program into point clouds could facilitate frequent nationwide forest inventory updates, as was discussed by Strunk et al. (2019) in a related study. Biennial nationwide inventory updates from lidar may be preferable to DAP, but are simply not viable given the current cost of lidar.

Despite the stark visual differences between point clouds from the multiple datasets we used in this study, our results showed that selected forest attributes known to correlate highly with tree height can be measured effectively regardless of the resolution (7.5 cm, 15 cm, 30 cm frame camera, and 40 cm pushbroom sensor). This agrees with other studies which have compared multiple DAP datasets and found that the results were fairly insensitive to variations in the acquisition parameters (Bohlin et al., 2012; Gobakken et al., 2015; Nurminen et al., 2013). While our results indicated that metrics computed from pushbroom DAP fared measurably worse than from a frame camera for ABA, our results also suggest that pushbroom DAP is still effective in explaining variation in forest attributes. We are not aware of another study which has contrasted frame-based DAP with pushbroom DAP and lidar all from an airborne platform, but our findings contribute to the body of literature which indicates that DAP from a wide variety of sensors and platforms can be used effectively to measure forest attributes. Examples include small-format drone platforms (Puliti et al., 2015), large-format aerial frame cameras (Bohlin et al., 2012; Järnstedt et al., 2012), aerial pushbroom sensors (Pitt et al., 2014; Strunk et al., 2019), and satellite-based sensors (Immitzer et al., 2016; Pearse et al., 2018; St-Onge et al., 2008; Vastaranta et al., 2014).

4.5. Limitations

One of the limitations of this study is the scope of our inferences with respect to broad usage of pushbroom imagery, specifically Leica ADS100 pushbroom imagery. Our results for Washington State have proven particularly good relative to what other users have encountered in other parts of the country with imagery from the same sensor. Very preliminary investigations (not shown) suggest that rather than attributing this to differences among acquisitions, it is likely that our use of BAE Socet by a highly qualified photogrammetrist with extensive experience tuning the software has resulted in a specialized product that we have been unable to obtain elsewhere. The software has a steep learning curve and is extraordinarily slow when processing large areas. The vendors of ADS100 imagery have found it difficult and expensive to generate a reliable point cloud for forestry purposes with this and other software, and have been less tolerant of the long durations required for processing pushbroom imagery with Socet. Frame-based imagery, in contrast, is much easier and more reliable to process.

Another limitation of this study is that there may be other ways to leverage point clouds which would be more or less impacted by acquisition configuration. Individual Tree Detection (ITD) especially is likely to be impacted by resolution and data source, where some ITD methods would be impacted by the lack of points beneath the canopy. Similarly, voxel-based approaches could be quite different as a function of sensor type and collection parameters.

A final limitation is that this study did not consider image overlap. Greater image overlap increases the continuity of the scene representation and typically yields fewer point cloud artifacts. In our study, frame camera imagery used only 30% sidelap, and no sidelap was used with pushbroom imagery. However, minimal overlap specifications are common in imagery collected to support the generation of orthophotos. Opportunistic use of this imagery for alternative purposes, such as point cloud product, can be attractive owing to their low cost, but will likely have similar overlap specifications.

5. Conclusions

Interest in DAP for forest inventory is growing due to its low cost and the fact that it can be used to model selected forest attributes nearly as well as lidar. This study compares results from multiple resolutions of data and imagery and from multiple sensor types to further evaluate the effectiveness of DAP. We confirmed what has been found in other studies that DAP is slightly inferior to lidar for modeling forest attributes, and that the results were fairly insensitive to image resolution (15 cm to 40 cm). Although frame-based DAP was slightly superior to pushbroom DAP, the results indicate that DAP from both frame and pushbroom sensors can be used effectively to support area-based forest inventory even with relatively low overlap and moderate resolution (30–40 cm). This is encouraging for the potential to enable forest inventory over large areas with pushbroom imagery, but further work is needed to create a DAP workflow with pushbroom imagery that is both suitable for forest inventory and scalable to rapid processing for large areas.

Funding

This research did not receive any specific grant from funding agencies in the public, commercial, or not-for-profit sectors.

Declaration of competing interest

The authors declare that they have no known competing financial interests or personal relationships that could have appeared to influence the work reported in this paper.

Acknowledgements

We would like to thank Washington State DNR for initiating this research study, and for their willingness to share the resulting field measurements and remote sensing data with us. Thank you also Hans-Erik Andersen and David Bell from the USFS VMaRS team for discussions and for revisions and contributions to an early draft. Finally we would like to thank three generous reviewers for their time, energy, and insights which greatly improved this manuscript.

References

St-Onge, B., Hu, Y., Vega, C., 2008. Mapping the height and above-ground biomass of a mixed forest using lidar and stereo Ikonos images. Int. J. Remote Sens. 29, 1277–1294. https://doi.org/10.1080/01431160701736505.

Agisoft Photoscan Professional Edition, 2019. Agisoft, L.L.C.

Allen, C.D., Macalady, A.K., Chenchouni, H., Bachelet, D., McDowell, N., Vennetier, M., Kitzberger, T., Rigling, A., Breshears, D.D., Hogg, E.T., 2010. A global overview of drought and heat-induced tree mortality reveals emerging climate change risks for forests. For. Ecol. Manag. 259, 660–684.

Anderegg, W.R.L., Kane, J.M., Anderegg, L.D.L., 2013. Consequences of widespread tree mortality triggered by drought and temperature stress. Nat. Clim. Chang. 3, 30–36.

https://doi.org/10.1038/nclimate1635.
Bohlin, J., Wallerman, J., Fransson, J.E.S., 2012. Forest variable estimation using photogrammetric matching of digital aerial images in combination with a high-resolution DEM. Scand. J. For. Res. 27, 692–699. https://doi.org/10.1080/02827581.2012.686625.
Core Team, R., 2018. R: A Language and Environment for Statistical Computing.
Flewelling, J.W., 1994. Stem Form Equation Development Notes. Northwest Taper Cooperative.
Furnival, G.M., Wilson Jr., R.W., 1974. Regressions by leaps and bounds. Technometrics 16, 499–511.
Furukawa, Y., Ponce, J., 2010. Accurate, dense, and robust multiview stereopsis. IEEE Trans. Pattern Anal. Mach. Intell. 32, 1362–1376.
Gobakken, T., Bollandsås, O.M., Næsset, E., 2015. Comparing biophysical forest characteristics estimated from photogrammetric matching of aerial images and airborne laser scanning data. Scand. J. For. Res. 30, 73–86. https://doi.org/10.1080/02827581.2014.961954.
Haavik, L.J., Billings, S.A., Guldin, J.M., Stephen, F.M., 2015. Emergent insects, pathogens and drought shape changing patterns in oak decline in North America and Europe. For. Ecol. Manag. 354, 190–205.
Immitzer, M., Stepper, C., Böck, S., Straub, C., Atzberger, C., 2016. Use of WorldView-2 stereo imagery and National Forest Inventory data for wall-to-wall mapping of growing stock. For. Ecol. Manag., Special Section: Forests, Roots and Soil Carbon 359, 232–246. https://doi.org/10.1016/j.foreco.2015.10.018.
Iqbal, I.A., Musk, R.A., Osborn, J., Stone, C., Lucieer, A., 2019. A comparison of area-based forest attributes derived from airborne laser scanner, small-format and medium-format digital aerial photography. Int. J. Appl. Earth Obs. Geoinformation 76, 231–241. https://doi.org/10.1016/j.jag.2018.12.002.
Jactel, H., Petit, J., Desprez-Loustau, M.-L., Delzon, S., Piou, D., Battisti, A., Koricheva, J., 2012. Drought effects on damage by forest insects and pathogens: a meta-analysis. Glob. Chang. Biol. 18, 267–276.
Järnstedt, J., Pekkarinen, A., Tuominen, S., Ginzler, C., Holopainen, M., Viitala, R., 2012. Forest variable estimation using a high-resolution digital surface model. ISPRS J. Photogrammetry Remote Sens. 74, 78–84. https://doi.org/10.1016/j.isprsjprs.2012.08.006.
Kangas, A., Gobakken, T., Puliti, S., Hauglin, M., Naesset, E., 2018. Value of airborne laser scanning and digital aerial photogrammetry data in forest decision making. Silva Fenn. 52. https://doi.org/10.14214/sf.9923.
Kim, E., Lee, W.-K., Yoon, M., Lee, J.-Y., Son, Y., Abu Salim, K., 2016. Estimation of voxel-based above-ground biomass using airborne LiDAR data in an intact tropical rain forest. Brunei. Forests 7, 259. https://doi.org/10.3390/f7110259.
Kukkonen, M., Maltamo, M., Packalen, P., 2017. Image matching as a data source for forest inventory–comparison of Semi-Global Matching and Next-Generation Automatic Terrain Extraction algorithms in a typical managed boreal forest environment. Int. J. Appl. Earth Obs. Geoinformation 60, 11–21.
Kukkonen, M., Maltamo, M., Korhonen, L., Packalen, P., 2019. Comparison of multispectral airborne laser scanning and stereo matching of aerial images as a single sensor solution to forest inventories by tree species. Remote Sens. Environ. 231, 111208. https://doi.org/10.1016/j.rse.2019.05.027.
Mantgem, P.J. van, Nesmith, J.C.B., Keifer, M., Knapp, E.E., Flint, A., Flint, L., 2013. Climatic stress increases forest fire severity across the western United States. Ecol. Lett. 16, 1151–1156. https://doi.org/10.1111/ele.12151.
McGaughey, R.J., 2016. FUSION/LDV: Software for LIDAR Data Analysis and Visualization, Version 3.01. USFS.
McGaughey, R.J., Ahmed, K., Andersen, H.-E., Reutebuch, S.E., 2017. Effect of occupation time on the horizontal accuracy of a mapping-grade GNSS receiver under dense forest canopy. Photogramm. Eng. Remote Sens. 83, 861–868. https://doi.org/10.14358/PERS.83.12.861.
Millar, C.I., Stephenson, N.L., 2015. Temperate forest health in an era of emerging megadisturbance. Science 349, 823–826.
Nurminen, K., Karjalainen, M., Yu, X., Hyyppä, J., Honkavaara, E., 2013. Performance of dense digital surface models based on image matching in the estimation of plot-level forest variables. ISPRS J. Photogrammetry Remote Sens. 83, 104–115. https://doi.org/10.1016/j.isprsjprs.2013.06.005.
Pearse, G.D., Dash, J.P., Persson, H.J., Watt, M.S., 2018. Comparison of high-density LiDAR and satellite photogrammetry for forest inventory. ISPRS J. Photogrammetry Remote Sens. 142, 257–267. https://doi.org/10.1016/j.isprsjprs.2018.06.006.
Pitt, D.G., Woods, M., Penner, M., 2014. A comparison of point clouds derived from stereo imagery and airborne laser scanning for the area-based estimation of forest inventory attributes in boreal ontario. Can. J. Remote Sens. 40, 214–232. https://doi.org/10.1080/07038992.2014.958420.
Probst, A., Gatziolis, D., Strigul, N., 2018. Intercomparison of photogrammetry software for three-dimensional vegetation modelling. R. Soc. Open Sci. 5, 172–192.
Puliti, S., Ørka, H.O., Gobakken, T., Næsset, E., 2015. Inventory of small forest areas using an unmanned aerial system. Remote Sens. 7, 9632–9654. https://doi.org/10.3390/rs70809632.
Rothermel, M., Wenzel, K., Fritsch, D., Haala, N., 2012. SURE: photogrammetric surface reconstruction from imagery. In: Proceedings LC3D Workshop, pp. 2 Berlin.
Strunk, J.L., Reutebuch, S.E., Andersen, H.-E., Gould, P.J., McGaughey, R.J., 2012. Model-assisted forest yield estimation with light detection and ranging. West. J. Appl. For. 27, 53–59.
Strunk, J., Packalen, P., Gould, P., Gatziolis, D., Maki, C., Andersen, H.-E., McGaughey, R.J., 2019. Large area forest yield estimation with pushbroom digital aerial photogrammetry. Forests 10, 397. https://doi.org/10.3390/f10050397.
Thomas Lumley, 2017. Leaps: Regression Subset Selection Based on Fortran Code by Alan Miller.
Trimble Inpho, 2019. Trimble.
Vastaranta, M., Wulder, M.A., White, J.C., Pekkarinen, A., Tuominen, S., Ginzler, C., Kankare, V., Holopainen, M., Hyyppä, J., Hyyppä, H., 2013. Airborne laser scanning and digital stereo imagery measures of forest structure: comparative results and implications to forest mapping and inventory update. Can. J. Remote Sens. 39, 382–395. https://doi.org/10.5589/m13-046.
Vastaranta, M., Niemi, M., Karjalainen, M., Peuhkurinen, J., Kankare, V., Hyyppä, J., Holopainen, M., 2014. Prediction of forest stand attributes using TerraSAR-X stereo imagery. Remote Sens. 6, 3227–3246. https://doi.org/10.3390/rs6043227.
Walker, S., Pietrzak, A., 2015. Remote measurement methods for 3-D modeling purposes using BAE Systems' Software. Geodesy Cartogr. 64, 113–124.
White, J.C., Stepper, C., Tompalski, P., Coops, N.C., Wulder, M.A., 2015. Comparing ALS and image-based point cloud metrics and modelled forest inventory attributes in a complex coastal forest environment. Forests 6, 3704–3732. https://doi.org/10.3390/f6103704.
Wu, C., 2013. Towards linear-time incremental structure from motion. In: 2013 International Conference on 3D Vision-3DV 2013. IEEE, pp. 127–134.